Journal Name

ARTICLE TYPE

Cite this: DOI: 10.1039/xxxxxxxxxx

Self-Trapping Relaxation Decay Investigated by Time-Resolved Photoelectron Spectroscopy

Aude Lietard,[a] Giovanni Piani,[a] Marc Briant,[a] Marc-André Gaveau,[a] Sylvain Faisan,[b] Vincent Mazet,[b] Benoît Soep,[a] Jean-Michel Mestdagh,[a] and Lionel Poisson *[a]

Received Date
Accepted Date

DOI: 10.1039/xxxxxxxxxx

www.rsc.org/journalname

The present work combines time-resolved photoelectron spectroscopy on isolated species with high-level data processing to address an issue, which usually pertains to material science: the electronic relaxation dynamics towards the formation of a Self-Trapped Exciton (STE). Such excitons are common excited states in ionic crystals, silica and rare gas matrices. They are associated with a strong local deformation of the matrix. Argon clusters were taken as a model. They are excited initially to a Wannier exciton at 14 eV and their evolution towards the formation of a STE has showed an unusual type of vibronic relaxation where the electronic excitation of the cluster decreases linearly as a function of time with a 0.59 ± 0.06 eV $\cdot$ ps^{-1} rate. The decay was followed for 3.0 ps, and the STE formation occurred in $\sim 5.1 \pm 0.7$ ps.

1 Introduction

The efficiency of photoconverter cells, both in biological media [1] and in anthropogenic analogues (*e.g.* photovoltaic cells [2]) is very much controlled by the relaxation dynamics of excitons. Exciton formation is indeed essential to carry the light excitation onto the active centre where charges are created. The production of charges is also inherent to exciton formation and relaxation. An important point from the application point-of-view is that the exciton dynamics is often associated with material-free transport mechanisms, hence providing the relevant devices with a remarkably high fatigue resistance. This has motivated a considerable activity to unravel the relaxation dynamics of excitons in finite nanoscale materials [3]. Nevertheless, its thorough understanding is not at hand, yet. We consider that a breakthrough in this domain may emerge from novel experimental informations where the exciton dynamics is followed using dedicated tools of proved efficiency in unraveling complex dynamics of gas-phase isolated species (organic and bio-organic molecules, atomic and molecular clusters), where an interplay exists between electronic and geometrical degrees of freedom [4,5].

The present work aims at addressing experimentally the question of exciton formation, in isolated gas phase species. A time-resolved approach is used to describe the evolution of the initially excited state to a self trapped state. The formation of such a so called molecular Self-Trapped Exciton (m-STE) is commonly observed in rare gas solids as well as in alkali halides crystals [6]. In both medias, when an electron is promoted to a higher state, dimerization is observed for both systems, in accordance to their isoelectronic structures. Indeed, Cl_2^- is isoelectronic to Ar_2^+ and their formation creates a strong reorganization of the lattice. Both ions have a strong molecular behaviour [7,8] whereas their interactions in the ground state are dominated by van-der-Waals or electrostatic interactions. As a consequence, none of these relaxed ionic molecules can be created by a Franck-Condon transition. Their formation is the result of a relaxation process within the material.

STE formation was studied by time-resolved absorption spectroscopy [9] in silica and ionic crystals. Here, we propose an exploratory investigation of a m-STE formation in a model material that can be brought in the gas phase: nanometer size argon clusters, where easily distinguishable dynamical effects are expected. Ultrafast lasers are associated with powerful gas phase characterization tools. This allows conducting time-resolved photoelectron and photoion spectroscopies experiments within a pump-probe scheme. Accordingly, an exciton wavepacket is created within an argon cluster and its dynamics is monitored as a function of time with femtosecond resolution.

The current knowledge of surface and bulk excitons in materials formed of heavy rare gases relies on pioneering works performed in cryogenic matrices [10,11] and rare gas clusters [12,13]. A broad exciton band peaking near 14 eV was observed in argon clusters and assigned to overlapping Franck-Condon Wannier-type exciton states [13], nearby the ionisation energy. The present work reports the dynamics initiated from the excitation of this particular exciton state to the formation of a final STE with

[a] *LIDYL, CEA, CNRS, Université Paris-Saclay,CEA Saclay 91191 Gif-sur-Yvette France. E-mail: lionel.poisson@cea.fr*
[b] *ICube, Université de Strasbourg, CNRS,300 boulevard Sébastien Brant, BP 10413, 67412 Illkirch,France.*

an Ar_2^* core. Relaxation products of this type of STE were observed in other groups as reported for example by Hirayama and Arakawa.[14]

2 Experimental Setup

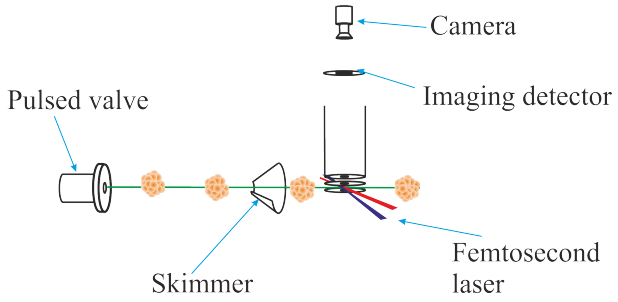

Fig. 1 Experimental setup.

The experimental setup used for this study is schemed in Fig. 1 and described more extensively elsewhere[15,16]. Shortly, argon clusters are generated in the source chamber by a pulsed supersonic expansion of pure argon in vacuum. Under the present conditions (100μm nozzle diameter; room temperature; 16 bars stagnation pressure) the reduced condensation[17,18] parameter Γ^* is $\sim$2800 implying an average size of $\sim$500 atoms for the clusters[19]. The cluster beam is skimmed before entering the chamber of experiment where it crosses the pump and probe laser beams.

The laser beams are provided by the SLIC/LUCA laser facility (http://iramis.cea.fr/slic/PresentationSlic.php). The latter is based on an amplified Ti:Sapphire oscillator which delivers 2 mJ pulses at 796.5 nm with a repetition rate of 20 Hz and an optimal pulse duration of $\sim$50 fs. An adjustable fraction of this light is used to pump an UV-beamline. It is doubled collinearly in a BBO Crystal before being mixed with the fundamental beam. This delivers the third harmonic of the laser at $\sim$265.5 nm with a pulse duration of $\sim$100 fs. The UV pulse energy can be as large as 250 μJ when all the available laser energy is used for its generation. This regime serves for the single-color experiments reported in Sec. 3.1.1. In contrast, the UV pulse energy is maintained to 100 μJ, typically, in the two color experiments reported in Sec. 3.1.2. Under this regime, it serves for the 3-photon pump excitation mentioned below in the paper. The remaining fundamental light (IR-beamline) of the Ti:Sapphire irradiates the excited clusters and probes them by ionization, after passing through an adjustable delay line. The pump laser is focused on the argon cluster beam, whereas the probe laser is slightly out of focus. The irradiance in the laser interaction region are 5.10^{13}W.cm^{-2} (265.5 nm) and 2.10^{12}W.cm^{-2} (796.5 nm). The corresponding ionization probability of an argon atom is 3.10^{-5} and $< 1.10^{-7}$, respectively, according to the ADK model[20,21]. Extrapolation to argon clusters of 500 atoms, assuming no transient absorption, leads to an ionization probability of a few percent. This order of magnitude is consistent with the ionization signal observed in the present experiment. Such irradiance values may be considered as unreasonably high with regards to standard pump/probe spectroscopy of molecules. However, it is unavoidable in the current context, considering the very small ionization probability of the argon target.

The resulting photoelectrons are collected using a Velocity Map Imaging Spectrometer[22] which monitors their velocity distributions. The 3-dimension electron distributions are extracted from the 2-dimension images by an inverse Abel Transform using the pBASEX technique[23]. The isotropic component of the photoelectron distribution only is considered here. It allows us constructing photoelectron spectra as reported in Fig. 3. The energy resolution is $\Delta E/E = 4\%$ at 3 eV.

3 Results

3.1 Experimental data

3.1.1 Single-color experiments

Figure 2 presents a raw image collected when the argon clusters interact with 265.5 nm UV-pulses of maximum energy (250 μJ). The image is summed over 3000 laser shots. The corresponding photoelectron spectrum is shown on the right side of Figure 2. Three contributions labeled R1, R2 and R3 appear in the figure. The R1 contribution is centred slightly below 3 eV electron energy. It is associated with a non-resonant 4-photon ionization ([4+0]) of isolated argon atoms, *i.e.* argon atoms which are not bound to clusters (Ionization Energy of isolated Ar atom: 15.759606 ± 0.000009 eV[24]). The spin-orbit splitting of 0.18 eV of the Ar^+ ion appears as a shoulder in the R1 contribution (compare the experimental signal and the purple curve in the right panel of Figure 2). This contribution accounts for about 25% of the total signal. The remaining 75% is due to the ionization of argon clusters. They show up as R2 and R3. Contribution R2 is consistent with the direct ionization process of argon clusters (another [4+0] photon process). The Ionization Energy threshold (aIE) associated with R2 is measured indeed at 14.30 ± 0.05 eV, in agreement with previous measurements[25]. The green lines drawn within the experimental spectrum above 4 eV electron energy show how this threshold was extracted. The vertical Ionization Energy (vIE) can be estimated as 14.70 ± 0.1 eV when identified to the photoionization energy where the maximum photoelectron emission is observed. This is in reasonable agreement with what can be deduced from Refs[25,26]. Elastic scattering of the ejected electron[27] within the cluster is likely to randomize their trajectories. This makes the electron angular distribution fairly isotropic as revealed by the unpolarized R2 contribution observed in the left panel of Figure 2. Such depleted polarization was partially observed with deposited molecules or atoms on clusters[28]. It seems to be even more pronounced for electrons that are ejected out of the core of the cluster.

Contribution R3 documents electron of very low kinetic energy. The latter electron component is best observed in the top-right panel of Figure 2. The origin of these cold electrons will be discussed later in the present paper and appears to be associated with a resonant [3+1] photon process.

3.1.2 Two-color experiments

In the previous section, 100% of the IR-pulse energy was used to generate the UV-pulse. In the present section, only a fraction of the IR-pulse energy is used to generate the UV-pulse. It

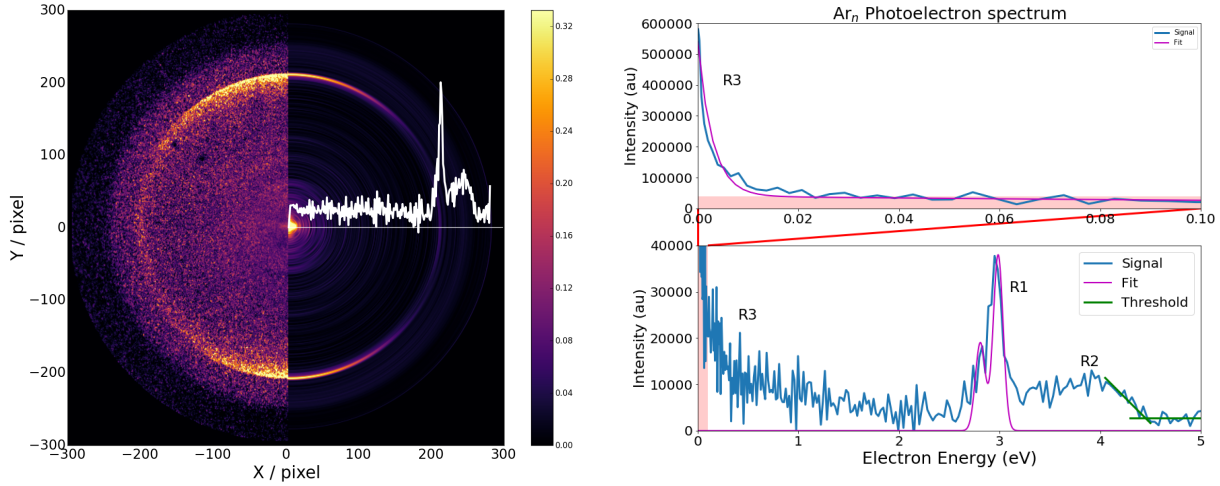

Fig. 2 [Left] Photoelectron image collected when irradiating the argon clusters at 265.6 nm with a pulse energy of 250 μJ (maximum available energy). The electron are generated by a 4-photon process, either [4+0] or a [3+1] as explained in the text. The laser is polarized vertically with respect to the image, which has therefore a up-down and right-left symmetry. The left side of the image is a raw image where the signal is simply multiplied by the radius. This emphasizes the contribution electrons with large kinetic energy. The right side of the image is an inverted image, also with the signal multiplied by the radius. The resulting velocity distribution is superimposed in white. [Bottom Right] Corresponding photoelectron spectrum (blue). The purple curve is the fit of the expected photoelectron band for the ionization of isolated argon atoms (R1), taking into account the laser bandwidth. The green lines underline the energy threshold for the ionization of clusters (R2). [op right] expansion of the energy scale and contraction the intensity scale of the bottom-right panel to make apparent the R3 component of low energy electrons. The pink regions figure out the overlap between the two spectra.

is then possible to irradiate the clusters with both UV-pulses and IR-pulses and to tune the relative energy between these pulses. Accordingly, the efficiency of the 4-photon ionization processes observed in the previous section is maintained at the lowest level. With a careful adjustment of the UV and IR-pulse energies another ionization process is superimposed to that observed above. It is a multiphoton two color ionization process where a non resonant three 265.5 nm-photon (14.0 eV) excitation of the cluster is followed by either a single or a two IR-photon ionization of the electronically excited cluster. Since the UV and IR-pulses can be delayed in time, this allows performing a femtosecond pump-probe study where $Ar_{\approx 500}$ clusters[19] are excited by the pump within the 14 eV exciton band. Pump schemes involving a different number of photons can be ruled out. No absorption band is reported indeed on argon clusters near the energy of one or two 265.5 nm-photons. This precludes as well the multi-absorption of one or two non resonant UV photons. Also, the energy of four UV photons is above the ionization energy of $Ar_{\approx 500}$ and the resonant absorption of four photons ([3+1]) leads to the ionization signals observed in the previous section. The latter process is much more favorable than multi-absorption of 3 non-resonant UV photons by the same cluster, therefore excluded. Furthermore, no noticeable evolution in the shape of the signal of interest was observed when changing the energy balance between the UV and IR-pulses. Note however that the range where this balance can be changed is rather narrow. The UV-pulse energy cannot be too low to keep the 3-photon pump signal detectable but cannot be too high, otherwise the 4-photon ionization processes would overwhelm the pump-probe signal.

Given the above analysis, the clusters are excited electronically by the pump within the 14 eV exciton band. They are probed at 795.5 nm in a 1- (1.56 eV) or 2-photon (3.12 eV) ionization process. The time resolved photo-electron spectroscopy technique[29] is used to document the relaxation dynamics of the initial electronic excitation. Fig. 3 displays the corresponding photoelectron spectra as a function of the pump-probe delay up to 4.0 ps. The contribution of single color signals is removed from all the displayed spectra by substraction of the averaged spectra collected before the laser cross correlation. Additional experiments were conducted at larger time delays, up to several hundreds of ps. They document the delayed evaporation of $Ar^\star$ and $Ar_2^\star$ from the cluster, which appears after the initial exciton has relaxed. These observations agree with those of Hirayama and Arakawa [14] in matrices and will be published in a separate paper.

Three observations can be done on Fig. 3. First, a broad, very intense band extending between 0 and *ca* 1.2 eV appears near the zero time delay during the cross correlation time of the lasers. As appears this band has a low intensity replicate between 1.2 and 2.5 eV. Second, a band of low energy (0-0.15 eV) and a very diffuse background band (0.15-1.3 eV) appears slowly after the laser cross correlation. These bands reach a plateau after 1.5 ps and 2.5 ps time delay, respectively. Their position and width do not change significantly over the time range of the figure. The third observation is the focus of our attention hereafter: a fairly broad band distributed over a 0.8 eV width observed between zero and 1.5 ps time delays (lower dotted line on Figure 3). Its centre energy decreases linearly as the delay time is increased from zero to 1.5 ps. *In contrast, its intensity and width are fairly constant*. This behaviour is profoundly different from usual signals observed in time-resolved photoelectron spectroscopy, where the relative intensity of the photoelectron bands changes but not (or marginally) their position and width[30].

A secondary time-dependent band of very low intensity appears also in Fig. 3. It parallels the primary band described above, apparently with an offset of 1.56 eV in energy. This band probes likely the same wavepacket movement as the primary band, but it is associated with one more probe photon for ionization. Its intensity is close to the noise limit, nevertheless its observation will be useful because the additional probe photon allows documenting the energy relaxation on a wider energy range, 3 eV, instead of 1.5 eV with the primary band. Hereafter, these bands are called the *time-dependent bands*.

3.2 Data processing of the *time-dependent bands*

The quantitative analysis of photoelectron signals, where the band structure (intensity, centre or width) changes as a function of the time delay, requires specific data analysis techniques [15,31]. A Bayesian inference method is used here in a joint decomposition procedure where all the photoelectron spectra which served to construct Fig. 3 are decomposed simultaneously. This allows including continuity constraints in the prior distributions of the band parameters, hence favoring a smooth change of these quantities as a function of the delay time, even in situation where the signal/noise ratio is poor. Among the constraints that are given to the band parameters, one is that the width of the time-dependent bands is constant and another that their centres move linearly as a function of the time delay.

According to this data processing, the primary time-dependent band has a full width at half maximum (FWHM) of 0.47 ± 0.1 eV. Its centre, initially (zero time delay) at 1.0 ± 0.1 eV, goes down in energy at a rate of 0.59 ± 0.06 eV$\cdot$ps^{-1}. This band can be followed up to 1.5 ps time delay, as it merges into the low energy electron band which is growing up between 0 and *ca* 1.5 ps. This analysis also confirms that the secondary time-dependent band mentioned above has the same behaviour as the primary one, except it is shifted at higher energy by 1.56 eV (2 photon probe). Its centre goes therefore down in energy at the same rate as the primary band, between 2.56 eV at zero time delay and 0.8 eV at 3 ps time delay.

4 Discussion

The discussion focuses in turn on the single-color experiment (section 4.1) and on the energetics which prevails in the two-color experiment (section 4.2). The time-dependent bands observed in the two-color experiment are then assigned to a specific exciton dynamics (section 4.3) and finally a model is proposed to account for the very peculiar behavior of these bands (section 4.4).

4.1 Cold electrons in the single-color experiment

The contribution of the cold electrons (R3) to the photoelectron spectrum displayed in Figure 2 can be fitted by a narrow band with an exponentially decaying side of 3 ± 1 meV energy constant over a broad energy distribution extending up to 2 eV. When converted to temperature, the decay would correspond to a 35 ± 12 K thermal distribution. This value is comparable with the temperature of 32 ± 2 K which was measured by Farges *et al.* [32] for argon clusters of similar size as those used here.

Ionization of clusters ejecting electrons at the cluster temperature was reported for the first time in the group of D. M. Neumark for helium-droplets [33,34]. In these works, the cold electron component represented 20% of the ejected electrons for ionization below the vIE. It was very small but measurable above this limit. This contribution was attributed to the autoionization of Rydberg states within the cluster.

In the present single-color experiment, the argon clusters are ionized with 4 UV-photons, *i.e.* with 18.7 eV. As seen earlier, the adiabatic ionization energy (aIE) of these clusters was measured at 14.30 ± 0.05 eV. The excess energy for the present 4-UV photon ionization of the cluster is therefore substantial and observing cold electron seems to be at odds with the results that have just been recalled for the helium droplets. The situation however is not fully comparable since the polarizability of argon is almost an order of magnitude larger than that of helium (1.64 *versus* 0.20 Å^3 [35]). Apparently this contributes to an efficient vibronic coupling that leads to the ejection of an electron from the excited cluster.

4.2 Energetics in the two-color experiment

The assignment of the two time-dependent bands is an important landmark of the discussion below (section 4.3). It is very much based on the energetics drawn in the present section. We first focus on the initial energy of these bands (section 4.2.1), then on the energy that the electronic energy of the cluster could reach at the end of the energy relaxation (section 4.2.2).

4.2.1 Initial energy of the primary time-dependent bands

From the data processing section (section 3.2 we know that at zero delay-time the centre of the primary band is located at 1.0 eV and that of the secondary band at 2.56 eV. The latter value is simply a shift by 1.56 eV of the former since the secondary band corresponds to ionization of the cluster with one more probe-photon than the primary band. The centre of the primary band at time zero is an information prior any relaxation has started within the cluster. It reflects directly the [3+1'] scheme of the two color pump (265.5 nm)/probe (796.5 eV) experiment. According to this scheme, 14.01+1.56=15.57 eV are available for the photoionization. Given the vertical (14.70 ± 0.1 eV) and adiabatic (14.30 ± 0.05 eV) ionization energies of the argon clusters that are derived in Section 3.1.1, a photoelectron band peaking at 0.87 eV and extending up to 1.27 eV is expected. This agrees reasonably well with the observation in Figure 3 and confirms the [3+1'] pump/probe scheme.

4.2.2 Expected energetics of the final relaxation product

The intense primary time dependent band observed in Figure 3 peaks at 1.0 eV at zero pump-probe delay time. Then the energy of the band centre decreases as a function of time. This suggests that the electronic excitation carried by the cluster also decreases as a function of time. The secondary time-dependent band, which is due to ionization with one more probe-photon allows following the decrease of the electronic excitation over a wider range of time delays than the primary band: up to 3 ps instead of 1.5 ps. The photoelectron energy decreases from 2.56 to 0.8 eV

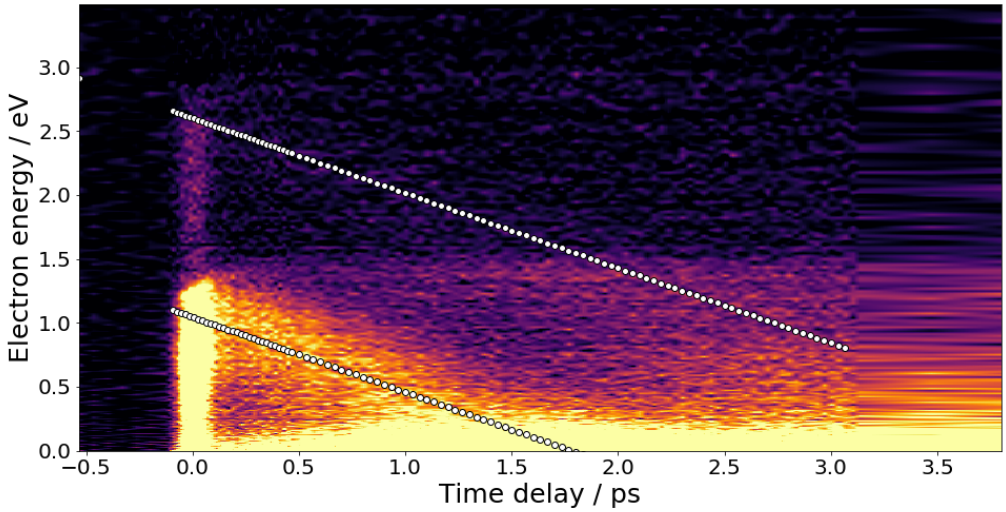

Fig. 3 Photoelectron spectra (vertical axis) *versus* the pump (265.5 nm) - probe (796.5 nm) time delay. The signal intensity is given in false colors with the same color code as in Figure 2. The contribution of the single-color signals either from the pump or the probe is removed as explained in the text. The white dotted lines show the fit of the two time dependent bands by the Bayesian inference method (see text).

when followed for 3 ps along the secondary time dependent band. This corresponds to a drop of the initial electronic excitation by 1.76 eV during this time window. Actually, a steady decrease of the electronic energy is observed along this band, with no indication that is goes asymptotically towards a plateau. Hence, the relaxation cannot be considered as completed over the 3 ps time window. Further clarification of this question is done below in the light of former works in the group to T. Möller on argon clusters and that of F. Spiegelman on the Ar_2 dimer.

Möller and coworkers documented the formation of exciton in argon clusters by monitoring their fluorescence emission as a function of the excitation energy[13]. The exciton of lowest energy was measured at 11.7 eV. The corresponding emission was dispersed for an excitation energy of 12.06 eV in the middle of the exciton band. Two bands are observed. One is centred at 9.72 eV and attributed to bulk emission and the other, centred at 11.38 eV, is assigned to surface emission[36]. Such a strong Stokes shift was interpreted as the formation of an Ar_2^* excimer within the cluster. This corresponds to a strong local modification of the cluster geometry, actually a m-STE, which traps the electronic excitation.

We infer that Ar_2^* excimer states are formed during the electronic energy relaxation, after the cluster has been excited within the 14 eV exciton band by the pump laser. The ionization properties of the Ar_2^* excimer states are reviewed now to check the reliability of this assumption.

Duplaa and Spiegelmann documented theoretically the excited electronic states of the Ar_2 dimer[37]. As a first approximation, these states can be considered as those of a diffuse Rydberg electron moving in the electric field of a compact ionic core Ar_2^+. With this picture in mind, the solvation energy of electronically excited Ar_2 is probably close, although slightly smaller, to that of Ar_2^+. The ionization energy of $Ar_2^\star$ within the cluster is thus expected to be close to the ionization energy of free $Ar_2^\star$. The latter is deduced below by combining the calculations of Duplaa and Spiegelmann on the Ar_2 dimer with asymptotic energies of $Ar + Ar^+$ [38].

The calculations of Duplaa and Spiegelmann show that the potential energy of the electronically excited Ar-Ar pair is described by a dense network of curves with many avoided crossings between the repulsive and attractive ones (see FIG. 1 of the Duplaa and Spiegelmann[37]). The diabatic attractive curves that can be built by hand on this network confirm the above picture. However they are not fully parallel to the Ar_2^+ potential curve. As a result, the Ar-Ar binding energies which are deduced from these curves are systematically smaller than the binding energy of Ar_2^+ (measured to 1.3136 eV[8]). For example, the binding energy along the diabatic $^3\Sigma_u^+$ curve which correlates to $Ar + Ar^\star(3p^5 4s)$ is ≈0.8 eV and that along the curves $^3\Pi_g^+$ correlating with $Ar + Ar^\star(3p^5 4p)$ is ≈1.0 eV. They are smaller than the binding energy of Ar_2^+ by ≈0.5 and ≈0.3 eV, respectively. From the NIST Atomic Spectra Database, the threshold ionization energy of the $Ar^\star(3p^5 4s)$ and $Ar^\star(3p^5 4p)$ levels is 4.21 and 2.48 eV, respectively. Given the binding energy of $Ar_2^\star$ compared to that of Ar_2^+, threshold ionization energies of ≈4.21-0.5=3.71 eV and ≈2.48-0.3=2.18 eV are estimated for the excited cluster that will be label as $Ar_n^\star(3p^{-1} 4s\ ^3\Sigma_u^+)$ and $Ar_n^\star(3p^{-1} 4p\ ^3\Pi_g)$ in the following.

Two probe photons provide $2 \times 1.56 = 3.12$ eV energy. With this probe scheme, $Ar_n^\star(3p^{-1} 4p\ ^3\Pi_g)$ can be ionized within the cluster with an excess energy of 0.94 eV, whereas the $Ar_n^\star(3p^{-1} 4s\ ^3\Sigma_u^+)$ excited cluster of lowest energy cannot be detected. This is schemed in Figure 4. Importantly the energy of 0.94 eV is reached along the secondary time dependent band after a ≈ 2.5 ps evolution time. The picture that emerges is the following: the time dependent bands relates to the formation of an $Ar_2^\star$ excimer embedded in the argon cluster, and presumably the cluster has relaxed its electronic energy down to a state correlating with $Ar_n^\star(3p^{-1} 4p\ ^3\Pi_g)$ in a 2.5 ps delay time. Likely, the excitation keeps relaxing within the cluster, beyond the 0-3 ps time window of the experiment and reaches the excimer level of lowest energy, $Ar_n^\star(3p^{-1} 4s\ ^3\Sigma_u^+)$. Since the pump excitation (14.0 eV) is 0.7 eV

below the vertical ionization of the clusters (14.7 ± 0.1 eV) and the ionization energy of $Ar_n^*(3p^{-1}\,4s\ ^3\Sigma_u^+)$ is 3.71 eV, this would correspond to an energy relaxation of $3.71 - 0.7 \pm 0.1 = 3.0 \pm 0.1$ eV. This relaxation is schemed by the green arrow in Figure 4.

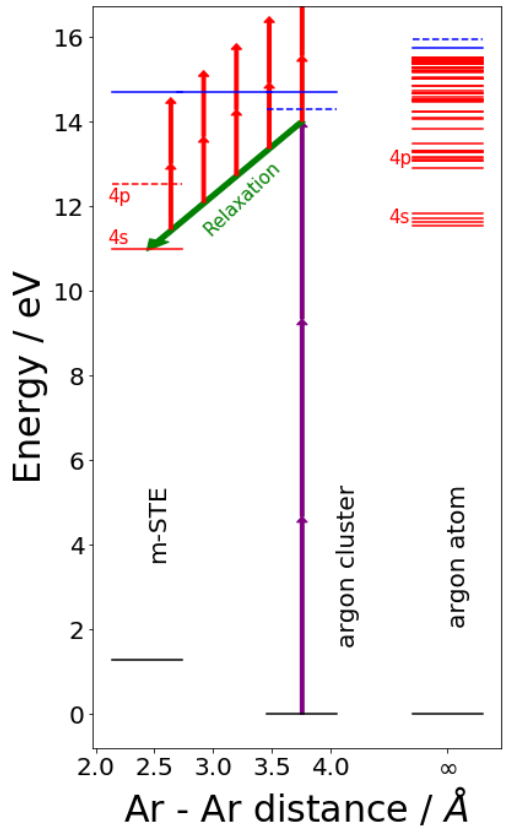

Fig. 4 Energy scheme of the system. The X axis schemes the $Ar - Ar$ distance along a process where this distance switches from its value in an argon matrix to that in the Ar_2^+ ion. [black] Ground state [blue] Ionic states (vIE). In dash blue for argon is the spin-orbit spliting, for the cluster, the aIE [red line] Excited states. For argon, only the s and p electronic configurations up to the $Ar^*(3p^5\,9p)$ are reported. For the shortest distance, the energy levels are estimated based on the hypothesis described in the text. [purple arrow] shows the pump laser energy; [red arrow] shows the probe laser energy.

4.3 Assignment of the time dependent bands to the dynamics of specific excitons

T. Möller and coworkers discussed the nature of the Franck-Condon exciton bands in argon clusters [12,13,39,40]. These authors found that the exciton band of lowest energy ($n = 1$) is built from the excitation of an argon atom to the 4s/4p Rydberg orbitals. Its energy variation with the cluster size is consistent with a spatially localized Frenkel exciton. In contrast, the $n \geq 2$ exciton bands which form the 14 eV band - where the present work initiates the dynamics - are of the Wannier-type. They have a large radius which scales as n^2: 7.2 Å and 16.2 Å for $n = 2$ and $n = 3$ respectively. For these extended excitons, a distinction must be made between surface and bulk excitons. The minimal radius for a cluster to carry a bulk exciton is 2-3 times the radius of the exciton [40].

4.3.1 Nature of the excitons formed by the initial 14 eV excitation

The present experiment is performed with $Ar_{\approx 500}$ clusters. Their average radius is estimated to *ca* 16 Å assuming an $Ar - Ar$ distance of 3.76 Å [41] and a compactness of 74%. From the indication above, the 14 eV excitation provided by 3-pump photons (bandwidth *ca* 60 meV) forms a complex $n \geq 2$ exciton wavepacket where the $n = 2$ exciton is a bulk Wannier exciton and the excitons of higher rank ($n > 2$) are confined Wannier excitons.

4.3.2 Evolution of the initial exciton wavepacket

After it was formed in the Franck-Condon region by the pump-laser, the wavepacket propagates and moves out of this region. This induces changes in the structure of the cluster which prevent the wavepacket to come back to the Franck-Condon region. We saw in Section 4.2.2 that at long delay time (3 ps) the energy of the wavepacket is adequately described by an excited state correlating with $Ar + Ar^*(3p^5\,4p)$ at infinite separation between the two Ar atoms. This fits with the observation of Möller and coworker that is recalled above: the exciton band of lowest energy ($n = 1$) is built from an argon atom in the 4s/4p Rydberg orbitals. For this reason we consider that the wavepacket which is probed by the time-dependent bands converges towards a Frenkel-type exciton, carried by an Ar_2^* excimer within the cluster. It is a m-STE. The dynamics which is observed over the 3 ps time-delay range thus corresponds to the switch from initial Wannier excitons to a final m-STE.

4.4 Information brought by the linear energy decrease observed on the time-dependent bands

We already mentioned that the present observation of photoelectrons, which decay continuously in energy as a function of the time delay, differs from the usual state-to-state signals observed in time-resolved photoelectron spectroscopy exhibiting a stepwise decrease of the energy of the electrons, related to the electronic states reached by relaxation. Nevertheless, a few examples have been reported where a continuous energy evolution of the electron energy was observed. This behaviour was found in the relaxation dynamics of species solvated in argon clusters [15,28] but there, the excitation was localized specifically on the solvated species and the electronic structure of the argon atoms was not involved in the dynamics. The observed smooth evolution of the electron spectra over only 0.14 eV was thought to document the geometrical reorganization of the argon atoms about the electronically excited centre. This energy shift is related to the gradual solvation of the excimer by the surrounding argon atoms. The ~ 2 ps loss of coherence in the relaxation of NO within argon matrices [42] shows that it corresponds to the relaxation time of argon clusters within matrices and emphasizes that coherence can be maintained for this duration in this medium.

The present situation is very different. With a confined Wannier-type exciton as initial state, the working picture is that of a quasi-free electron in the cluster together with the correspond-

ing hole that forms a molecular ionic core with the nearby Ar atoms. The Ar_2^+ binding energy, measured as 1.3136 ± 0.0008 eV[8] is large enough to justify such an association. As a result, both electronic and vibrational energy are deposited in the cluster by the pump laser pulse. Both are likely coupled during the subsequent relaxation. This picture precludes rationalizing the relaxation dynamics on the sole basis of nuclear motions as could be done in Refs.[15,28]. The key question is therefore to identify which description is most appropriate to account for the linear energy decrease.

4.4.1 Origin of the linear energy decrease

The linearly shifting band on the time resolved photo-electron spectrum in Figure 3 indicates that the electronic energy decreases linearly as a function of time. The Supplementary Information accounts for this behaviour by using a model which is broadly inspired by the network of curves calculated by Duplaa and Spiegelmann to describe the excited states of the Ar_2 dimer[37]. In fact, the model describes a more complex situation than suggested by the simple $Ar_2^\star$ potential curves. The accessible density of states is actually much larger given the large number of atoms over which the electronic energy can be delocalized at the beginning of the relaxation. This increases the dimensionality of the phase space and open additional relaxation channels through conical intersections. These topological singularities of the potential energy surface mix electronic and vibrational states as non-Born-Oppenheimer vibronic states. The large number of avoided crossings between the potential energy curves calculated by Duplaa and Spiegelmann[37] adds the symmetry breaking that induces the state mixing. This suggests that a very large number of coupling regions exist between adjacent states.

From the above considerations, the model that we propose features a large number of uniformly distributed states are considered. This mimics the large number of vibronic Rydberg states. In the simplest approximation, each state of the model is coupled to the two adjacent levels with the same coupling constant. This mimics the conical intersections coupling adjacent curves of the Duplaa and Spiegelmann work. The two model parameters (state density and coupling constant) are adjusted to reproduce the observed energy decrease of 0.59 ± 0.06 eV$\cdot$ps^{-1}. With this model, assuming that the electronic energy decays by 3.0 ± 0.1 eV as stated in section 4.2.2, the formation time of the m-STE could be estimated to $\sim 5.1 \pm 0.7$ ps of which, the only first 3 ps could be observed within the time window of the present experiment.

4.4.2 Various models of interpretation

Excitonic bands in nanometric particles are usually modeled as a compromise between a "delocalized atomic" (or "supermolecule") and a "confined electron-hole" (or "quasiparticle") point-of-view[3,43]. In the confined electron-hole approach, the interband relaxation is driven by the electron-phonon coupling whereas in the supermolecular approach, the coupling between electronic and vibrational wavepackets is considered explicitly.

Simply, the supermolecular picture leads to a description which localizes the excitation (the molecule) at the contact of a thermal bath (the molecular environment)[44] and is driven by the system-bath interaction, whereas in the confined electron-hole approach is based on the delocalization of the excitation.

In the present paper, the initial excitation is clearly delocalized (Wannier exciton), in definite contrast with the localization of the m-STE formed(Frankel exciton). Such situation is encountered when exciton delocalized states are mixed with local states, like in the reaction centers of photosynthetic systems[45] where exciton states are mixed with local charge transfer states. This assumes a generalized breakdown of the Born-Oppenheimer approximation along the dynamics and a picture based on a wavepacket moving on well identified potential energy surfaces is apparently no longer relevant. The confined electron-hole approach could be the appropriate approach to account for the initial vibronic relaxation (i.e. before the electronic excitation is localized on a single $Ar_2^\star$ molecule). Unfortunately, the present experimental information does not provide very much information on this aspect of the early dynamics. This will be the subject of a forthcoming paper where the energy and angular distribution of ejected species[14] from the cluster will be analyzed.

4.5 Cold electrons in the two-colors experiment

The above discussion concerns the electron bands whose centre energy varies as a function of the pump-probe delay. Other bands appear in Figure 3 that simply vary in intensity as the pump-probe delay is varied. In particular a band of low energy electron ($<$0.4 eV) is maximum near 1.2 ps delay time and slowly decreases above (the equivalent of band R3 in the single color experiment, see Section 4.1).

As seen in latter section, the ionization mechanism forming cold electrons proceeds from autoionization of internally excited clusters. Of course, its efficiency is enhanced when a resonant absorption is possible. In the present context of the two-color pump-probe experiment, a possible [3+1'] scenario is: first excitation by the pump at 14 eV, then autoionization by the probe laser in a resonant process, superimposed to the non-resonant process discussed in the previous sections. The maximum of this band at 1.2 ps time delay reflects the increased number of resonance states about the vertical ionization threshold.

5 Summary and conclusion

Argon clusters of $\sim$500 atoms were irradiated by three 265.5 nm photon within the 14 eV exciton band. They were detected along a one and a two photon ionization scheme in the near infrared (795.5 nm). This was performed within the framework of a femtosecond pump-probe experiment where energy and angular distribution of the photoelectron was recorded as a function of the pump/probe delay. This allowed us to document the time resolved relaxation dynamics of the electronically excited cluster from an initial superposition of bulk and confined Wannier exciton to the formation of a molecular Self-Trapped Exciton.

The picture that has emerged from the discussion is that of an initial wavepacket driven within a semi continuum of vibronic states. This leads to a dynamics where electronic and vibrational degrees of freedom are fully coupled. It is totally different from that of sequential decays between well separated states. In such

dynamics, the electronic energy varies suddenly when the system is hopping from one state to another, the populations of which decays exponentially as a function of time (*e.g.*[46,47]). The situation is entirely different here. The photoelectron energy which is monitored by the pump/probe experiment decreases linearly as a function of time. This evolution is followed for 3 ps. It indicates that the electronic energy of the clusters decreases also. An energy decrease of $0.59 \pm 0.06\ \mathrm{eV \cdot ps^{-1}}$ is observed and was interpreted quantitatively by a model where an initial wavepacket created by the pump laser moves through a bath of vibronic states.

The final state of the relaxation is assigned to a low lying Frenkel m-STE, presumably a $Ar_2^\star(^3\Sigma_u^+)$ excimer embedded in the cluster described diabatically by the $Ar + Ar^\star(3p^5 4s)$ configuration that could be reached in $\sim 5.1 \pm 0.7$ ps. However, the time window that is allowed by the probe laser energetics is limited to 3 ps. The present observations were discussed as consistent with the fact that during these 3 ps, the wavepacket which is moving in the dense network of vibronic states describing the $Ar_n^\star$ Rydberg states of the cluster has reached configurations in the same energy range as $Ar_n^\star(3p^{-1}\,4p\ ^3\Pi_g)$.

It is interesting to bring this picture of exciton dynamics within argon cluster together with an apparently related dynamics that was observed in helium droplets in the group of D. M. Neumark[48,49]. Actually, the situation in the helium droplet experiment is hardly comparable to the present one. First, the much larger size of the helium droplet does not confine the initial bulk Wannier exciton which, therefore, have a propagation degree of freedom that does not exist here. Second, the density of electronic states is much larger in the present argon experiment than in the helium one where only Σ-Potentiel Energy Surfaces (PES's) are involved. The mass of Helium which drives the dynamics is also an order of magnitudes smaller than the one of argon. This results into a more common state-to-state relaxation in helium droplet that is entirely different from that observed here.

Acknowledgments

The authors kindly thank Olivier Gobert, Michel Perdrix and Delphine Guillaumet for setting up and maintaining the SLIC/LUCA laser. LP acknowledges ANR11-EQPX0005-ATTOLAB for support. The authors thanks the CNRS for support under the grant "PEPS SPECTRODEC".

References

1 H. Lee, Y. C. Cheng and G. R. Fleming, *Science*, 2007, **316**, 1462–1465.
2 H. Hoppe and N. S. Sariciftci, *J. Mater. Res.*, 2004, **19**, 1924–1945.
3 G. D. Scholes and G. Rumbles, *Nat Mater*, 2006, **5**, 683–696.
4 A. Stolow and J. G. Underwood, in *Time-Resolved Photoelectron Spectroscopy of Nonadiabatic Dynamics in Polyatomic Molecules*, John Wiley and Sons Inc, New York, 2008, vol. 139, pp. 497–583.
5 A. Masson, L. Poisson, M. A. Gaveau, B. Soep, J. M. Mestdagh, V. Mazet and F. Spiegelman, *J. Chem. Phys.*, 2010, **133**, 054307.
6 R. T. Williams and K. S. Song, *J. Phys. Chem. Solids*, 1990, **51**, 679–716.
7 J. A. Ayala, W. E. Wentworth and E. C. M. Chen, *J. Phys. Chem.*, 1981, **85**, 768–777.
8 M. Briant, L. Poisson, M. Hochlaf, P. de Pujo, M.-A. Gaveau and B. Soep, *Phys. Rev. Lett.*, 2012, **109**, 193401.
9 S. Mao, F. Quéré, S. Guizard, X. Mao, R. Russo, G. Petite and P. Martin, *Applied Physics A*, 2004, **79**, 1695–1709.
10 V. Saile, M. Skibowski, W. Steinmann, P. Gurtler, E. E. Koch and A. Kozevnikov, *Phys. Rev. Lett.*, 1976, **37**, 305–309.
11 N. Schwentner, E. E. Koch and J. Jortner, *Electronic excitations in condensed rare gases*, Springer-Verlag, 1985.
12 T. Möller, *Z Phys D - Atoms, Molecules and Clusters*, 1991, **20**, 1–7.
13 J. Wormer, R. Karnbach, M. Joppien and T. Möller, *J. Chem. Phys.*, 1996, **104**, 8269–8278.
14 T. Hirayama and I. Arakawa, *J. Phys.-Condes. Matter*, 2006, **18**, S1563–S1580.
15 S. Awali, L. Poisson, B. Soep, M.-A. Gaveau, M. Briant, C. Pothier, J.-M. Mestdagh, M. B. E. H. Rhouma, M. Hochlaf, V. Mazet and et al., *Phys. Chem. Chem. Phys.*, 2014, **16**, 516.
16 L. Poisson, K. D. Raffael, M. A. Gaveau, B. Soep, J. M. Mestdagh, J. Caillat, R. Taieb and A. Maquet, *Phys. Rev. Lett.*, 2007, **99**, 103401.
17 O. F. Hagena, *Z Phys D - Atoms, Molecules and Clusters*, 1987, **4**, 291–299.
18 O. F. Hagena, *Rev. Sci. Instrum.*, 1992, **63**, 2374–2379.
19 S. Awali, M. A. Gaveau, M. Briant, J. M. Mestdagh, B. Soep, O. Gobert, R. Maksimenka and L. Poisson, *Phys. Chem. Chem. Phys.*, 2016, **18**, 32378 – 32386.
20 M. V. Ammosov, N. B. Delone and V. P. Krainov, *Zhurnal Eksperimentalnoi Teor. Fiz.*, 1986, **91**, 2008–2013.
21 X. M. Tong and C. D. Lin, *J. Phys. B*, 2005, **38**, 2593–2600.
22 A. Eppink and D. H. Parker, *Rev. Sci. Instrum.*, 1997, **68**, 3477–3484.
23 G. A. Garcia, L. Nahon and I. Powis, *Rev. Sci. Instrum.*, 2004, **75**, 4989–4996.
24 L. Minnhagen, *J. Opt. Soc. Am.*, 1973, **63**, 1185–1198.
25 F. Carnovale, J. B. Peel, R. G. Rothwell, J. Valldorf and P. J. Kuntz, *J. Chem. Phys.*, 1989, **90**, 1452–1459.
26 U. Hergenhahn, S. Barth, V. Ulrich, M. Mucke, S. Joshi, T. Lischke, A. Lindblad, T. Rander, G. Ohrwall and O. Bjorneholm, *Physical Review B*, 2009, **79**, 155448.
27 J.C. Gibson, R.J. Gulley, J.P. Sullivan, S.J. Buckman, V. Chan and P.D. Burrow, *J. Phys. B* , 1996, **29**, 3177–3195.
28 L. Poisson, E. Gloaguen, J.-M. Mestdagh, B. Soep, A. Gonzalez and M. Chergui, *J. Phys. Chem. A*, 2008, **112**, 9200–9210.
29 A. Stolow, A. E. Bragg and D. M. Neumark, *Chem. Rev.*, 2004, **104**, 1719–1757.
30 E. Gloaguen, J. M. Mestdagh, L. Poisson, F. Lepetit, J. P. Visticot, B. Soep, M. Coroiu, A. T. J. B. Eppink and D. H. Parker, *J. Am. Chem. Soc.*, 2005, **127**, 16529–16534.
31 V. Mazet, S. Faisan, S. Awali, M.-A. Gaveau and L. Poisson, *Signal Processing*, 2015, **109**, 193–205.

32 J. Farges, M. F. Deferaudy, B. Raoult and G. Torchet, *Surface Science*, 1981, **106**, 95–100.

33 D. S. Peterka, A. Lindinger, L. Poisson, M. Ahmed and D. M. Neumark, *Phys. Rev. Lett.*, 2003, **91**, 043401.

34 D. S. Peterka, J. H. Kim, C. C. Wang, L. Poisson and D. M. Neumark, *J. Phys. Chem. A*, 2007, **111**, 7449–7459.

35 P. Schwerdtfeger, in *Atomic Static Dipole Polarizabilities*, ed. G. Maroulis, Imperial College Press, 2006, pp. 1–32.

36 M. Joppien, F. Grotelüschen, T. Kloiber, M. Lengen, T. Möller, J. Wörmer, G. Zimmerer, J. Keto, M. Kykta and M. C. Castex, *Journal of Luminescence*, 1991, **48**, 601–605.

37 P. Duplaa and F. Spiegelmann, *J. Chem. Phys.*, 1996, **105**, 1500–1515.

38 Y. Ralchenko, A. E. Kramida, J. Reader and N. A. Team, *NIST Atomic Spectra Database (Version 3.1.4), [Online]. Available: HTTP://Physics.Nist.Gov/ASD3*, National Institute of Standards and Technology, Gaithersburg, MD, USA, 2008.

39 J. Wörmer, M. Joppien, G. Zimmerer and T. Möller, *Phys. Rev. Lett.*, 1991, **67**, 2053–2056.

40 J. Wormer and T. Möller, *Z. Phys. D*, 1991, **20**, 39–42.

41 E. Rühl, *Int. J. Mass Spectrom.*, 2003, **229**, 117–142.

42 C. Jeannin, M. T. Porrella-Oberli, S. Jimenez, F. Vigliotti, B. Lang and M. Chergui, *Chem. Phys. Lett.*, 2000, **316**, 51–59.

43 D. Abramavicius, B. Palmieri, D. V. Voronine, F. Sanda and S. Mukamel, *Chem. Rev.*, 2009, **109**, 2350–2408.

44 M. Khalil, N. Demirdoven and A. Tokmakoff, *J. Phys. Chem. A*, 2003, **107**, 5258–5279.

45 E. Romero, R. Augulis, V. I. Novoderezhkin, M. Ferretti, J. Thieme, D. Zigmantas, and R. van Grondelle, *Nat. Phys.*, 2014, **10**, 676.

46 S. Sorgues, J. M. Mestdagh, J. P. Visticot and B. Soep, *Phys. Rev. Lett.*, 2003, **91**, 103001.

47 A. Lietard, G. Piani, L. Poisson, B. Soep, J. M. Mestdagh, S. Aloise, A. Perrier, D. Jacquemin and M. Takeshita, *Phys. Chem. Chem. Phys.*, 2014, **16**, 22262–22272.

48 M. P. Ziemkiewicz, C. Bacellar, K. R. Siefermann, S. R. Leone, D. M. Neumark and O. Gessner, *J. Chem. Phys.*, 2014, **141**, 174306.

49 M. P. Ziemkiewicz, D. M. Neumark and O. Gessner, *Int. Rev. Phys. Chem.*, 2015, **34**, 239–267.